Propagation Model for Ultrafast Signals on Superconducting Dispersive Striplines

JOHN F. WHITAKER, STUDENT MEMBER, IEEE, ROMAN SOBOLEWSKI, DOUGLAS R. DYKAAR, THOMAS Y. HSIANG, MEMBER, IEEE, AND GERARD A. MOUROU

Abstract—**An algorithm suitable for the computer-aided design of transmission lines is used to model the propagation of picosecond and subpicosecond electrical signals on superconducting planar transmission lines. Included in the computation of a complex propagation factor are geometry-dependent modal dispersion and the frequency-dependent attenuation and phase velocity which arise as a result of the presence of a superconductor in the structure. The results of calculations are presented along with a comparison to experimental data. The effects of modal dispersion and the complex surface conductivity of the superconductor are demonstrated, with the conclusion that it is necessary to incorporate both phenomena for accurate modeling of transient propagation in strip transmission lines.**

I. INTRODUCTION

THE NEED TO increase the speed of response of many systems and components has led to great advances in the field of ultrafast, very high frequency electronics. Novel devices operating in the millimeter-wavelength range [1], [2] and new techniques for the generation and detection of electrical transients with terahertz bandwidth [3]–[6] have been designed. The progress in millimeter-wave integrated analog and digital circuits has led to the demand for a means to transmit waveforms of short duration from one location to another while maintaining fidelity. Since it has been discovered that it is difficult to propagate a signal with broad bandwidth on conventional striplines [7], [8], it is necessary to investigate variations on the design of transmission structures—such as the use of superconducting striplines—and understand how these designs affect electrical signals. From the circuit point of view, it is desirable to have a design tool developed which is capable of modeling these new transmission lines.

Manuscript received April 28, 1987; revised September 21, 1987. This work was supported in part by the United States Air Force Office of Scientific Research under Contract F49620-87-C-0016 to the Ultrafast Optical Electronics Center and by the National Science Foundation under Grant DMR-85-06689. Additional support of laser facilities was provided through the Laser Fusion Feasibility Project at the Laboratory for Laser Energetics of the University of Rochester, which has the following sponsors: Empire State Electric Energy Research Corporation, General Electric Company, New York State Energy Research and Development Authority, Ontario Hydro, and University of Rochester.

The authors are with the Ultrafast Science Center and the Department of Electrical Engineering, University of Rochester, Rochester, NY 14627. R. Sobolewski is also with the Institute of Physics, Polish Academy of Sciences, PL-02668, Warsaw, Poland.

IEEE Log Number 8717977.

The room-temperature study of broad-bandwidth waveform propagation in microstrip and coplanar transmission lines includes both experimental [8], [9] and theoretical work [10], [11]. Signal distortion, which can be quite serious for these lines, has been attributed mainly to two factors: a frequency-dependent propagation velocity due to modal dispersion, and a frequency-dependent attenuation due to the skin effect in the conductors.

The study of picosecond pulse propagation on superconducting transmission lines consists of a theoretical treatment for microstrip by Kautz [12] and experimental investigations on coplanar striplines by researchers at the University of Rochester [13], [14] and at IBM [15], [16]. These studies took into account the effect of the frequency dependence of the attenuation and phase velocity on a signal due to the complex surface conductivity of the superconductor. The results indicated a substantial signal attenuation only at frequencies above the energy gap. As opposed to the Rochester work [13], where dispersive transmission lines were studied, Kautz's calculations [12] neglected any dispersive behavior due to the line geometry, and the IBM reports [15], [16] argued that dispersion was insignificant because of the small dimensions of their structure. In all cases, improved transmission due to the almost lossless nature of the superconductor was evident, although the waveforms were still found to be distorted.

The contention of this paper is that superconducting transmission lines are vastly superior to normal-conduction media, and that to model accurately the propagation of ultrafast signals on these structures, one must consider modal dispersion and dielectric properties of the substrate, as well as the complex, frequency-dependent conductivity of the superconductor. We accomplish this goal through a comprehensive study of the transmission line propagation factor, and show that our model provides a very accurate, quantitative description of pulse propagation.

Our paper is organized as follows. Section II describes a practical algorithm for modeling transient propagation, including a general account of the characteristics of the transmission line and its frequency dependence due to geometry and to the presence of the dielectric substrate and superconductor. The details of the implementation of

0018-9480/88/0200-0277$01.00

the algorithm are presented in Section III, and examples of calculations for pulse propagation under different conditions appear in Section IV. Section V displays the outstanding agreement between the experimentally measured transients on a superconducting coplanar stripline and the calculations for that structure, while Section VI summarizes the work.

II. Description of the Transmission Line

The configuration under consideration is schematically shown in Fig. 1. A short, wide-band signal $V(\tau,0)$ is launched at the input of the transmission line ($z=0$), which is assumed to be long enough and/or is properly terminated such that reflections are not present. Under these conditions the propagated signal $V(\tau, z)$ at point z along the line can be evaluated, knowing $V(\tau,0)$ and several line properties: characteristic impedance Z_0 and complex propagation factor $\gamma(f)$. These quantities are defined in terms of the series impedance (Z) and shunt admittance (Y) per unit transmission line [17], [18]: $Z_0 = \sqrt{Z/Y}$ and $\gamma = \sqrt{ZY}$. By substitution we also find that $\gamma = Z/Z_0$. The propagation factor can also be divided into its real and imaginary parts:

$$\gamma(f) = \alpha(f) + j\beta(f) \tag{1}$$

where the real part is defined as attenuation and the imaginary component as a phase factor. The former is affected by conductor and dielectric losses, while the latter is mainly influenced by the line geometry (modal dispersion) and the conductor:

$$\alpha(f) \equiv \mathrm{Re}[\gamma(f)] = \alpha_d(f) + \alpha_c(f) \tag{2}$$

$$\beta(f) \equiv \mathrm{Im}[\gamma(f)] = \beta_{\mathrm{modal}}(f) + \beta_c(f). \tag{3}$$

If $\gamma(f)$ is precisely known, one can Fourier transform the input transient, $\boldsymbol{F}\{V(\tau,0)\}$, and "propagate" all frequency components along the line; the waveform, after propagating a distance z, is then recovered by taking an inverse Fourier transform of the resulting spectrum:

$$V(\tau, z) = \boldsymbol{F}^{-1}\left[\boldsymbol{F}\{V(\tau,0)\} \cdot \exp\{-\gamma(f) z\}\right]. \tag{4}$$

This scheme, together with a comprehensive computation of $\gamma(f)$, represents the essence of our modeling of the picosecond pulse propagation characteristics of the superconducting transmission line. It is clear that a successful, quantitative model must include all the physical mechanisms leading to the frequency dependence of the propagation factor. In the rest of this section the major factors contributing to $\gamma(f)$ will be reviewed.

For the coplanar striplines, the series impedance, with inductive and resistive contributions, and the shunt admittance, containing capacitive and conductive parts, are given as follows:

$$Z = j2\pi f \mu_0 g_1 + Z_s(f) g_2 \tag{5}$$

$$Y = 2\pi f \epsilon_0 \left(j\epsilon_r^{\mathrm{eff}} + \epsilon_r \tan\delta\right)/g_1 \tag{6}$$

where f is frequency, μ_0 and ϵ_0 are the permeability and permittivity of vacuum, $\tan\delta$ is the loss tangent of the substrate material, and $Z_s(f)$ is the conductor complex surface impedance described later. The effective permittivity $\epsilon_r^{\mathrm{eff}}$ is described in the next section, and ϵ_r is the relative permittivity of the substrate. The functions g_1 and g_2 depend upon the transmission line geometry and can be derived from design equations [19] (see the Appendix).

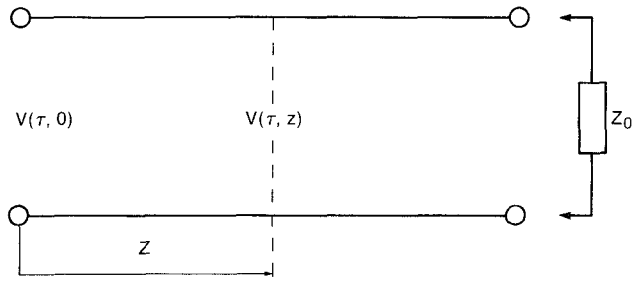

Fig. 1. Schematic diagram of transmission line, where $V(\tau,0)$ is signal input, and $V(\tau, z)$ is the output after propagation a distance z.

Throughout the paper we use the coplanar stripline as an example, although it should be realized that our conclusions are valid for any type of planar transmission line. The studies of other structures can be accomplished by simple modifications of several geometric parameters in the design equations. These changes can be easily implemented into the algorithm.

A. Modal Dispersion

The coplanar transmission lines (Fig. 2) are inherently dispersive—they cannot support a pure TEM wave [20]. The fringing electric field lines shown in Fig. 2 experience an inhomogeneous dielectric, leading to discontinuities in the field which cause contributions from longitudinal components. A closed-form expression for the effective permittivity encountered by a wave which is influenced by the substrate–superstrate interface was given for the coplanar geometry by Gupta *et al.* [19]:

$$\frac{\epsilon^{\mathrm{eff}}}{\epsilon_0} = \epsilon_r^{\mathrm{eff}} = \frac{\epsilon_r + 1}{2}\left[\tanh\left\{1.785\log\left(\frac{h}{w}\right) + 1.75\right\} + \frac{kw}{h}\left\{0.04 - 0.7k + 0.01(1 - 0.1\epsilon_r)(0.25 + k)\right\}\right] \tag{7}$$

where $k = s/(s+2w)$, and h, s, and w are defined in Fig. 2. Therefore, ϵ^{eff} (the subscript r will be subsequently omitted) for the coplanar stripline is an average of the permittivities from the dielectrics involved,[1] with the expression in the square brackets representing a correction term for the geometry of the line.

Strictly speaking, expression (7) is valid only when the wavelength of the radiation is much greater than the transverse dimensions of the stripline, when a quasi-TEM mode propagation may be assumed. As the wavelength

[1] Throughout this paper, we assume that the permittivity of the superstrate is equal to one.

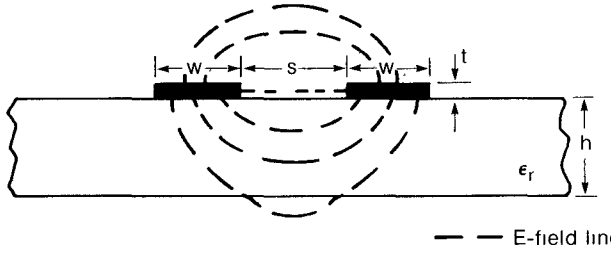

Fig. 2. Transverse cross section of coplanar stripline with representative electric-field lines shown.

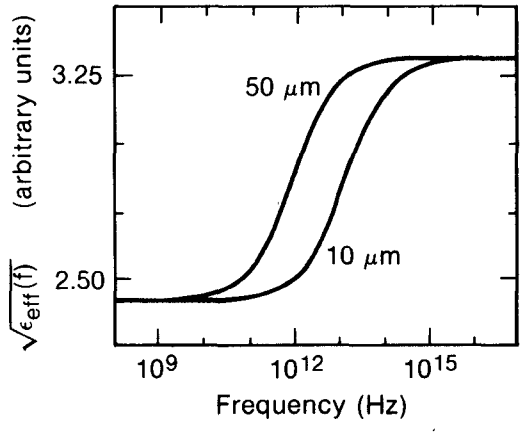

Fig. 3. Relative effective permittivity of coplanar striplines versus frequency. Both curves are for 1-mm-thick Si, while the step on the left is for a stripline with $w = s = 50$ μm and $t = 500$ nm, and the other has $s = 10$ μm, $w = 5$ μm, and $t = 300$ nm.

decreases and approaches the dimensions of the coplanar line, the longitudinal components on the line cause the effective permittivity to become frequency dependent. Full-wave analyses [21], [22] and semiempirical techniques [23], [24] have been employed to generate the dielectric function in microstrip lines. An approximate expression has been derived through curve fitting to the exact analysis [25], and extended by curve fitting to the dispersion data of coplanar waveguide [11] to give

$$\sqrt{\epsilon^{\text{eff}}(f)} = \sqrt{\epsilon^{\text{eff}}(0)} + \left[\frac{\sqrt{\epsilon_r} - \sqrt{\epsilon^{\text{eff}}(0)}}{1 + aG^{-b}}\right] \tag{8}$$

where $\epsilon^{\text{eff}}(0)$ is the quasi-static value given by (7), $G = f/f_{\text{TE}}$ is the normalized frequency, and

$$f_{\text{TE}} = c/\left(4h\sqrt{\epsilon_r - 1}\right) \tag{9}$$

is the cutoff frequency above which the first non-TEM mode enters in microstrip. The constants a and b depend on the line geometry. The result of (8) is shown versus frequency in Fig. 3 for two different coplanar striplines in order to demonstrate the change in permittivity with both frequency and geometry.

From this analysis we determine the contribution to the phase factor due to the modal dispersion. The phase velocity, defined as

$$v_\phi = 2\pi f/\beta(f) \tag{10}$$

can be combined with the equivalent expression for the velocity of propagation, $v = c/\sqrt{\epsilon^{\text{eff}}(f)}$, to give

$$\beta_{\text{modal}} = \left(\frac{2\pi f}{c}\right)\sqrt{\epsilon^{\text{eff}}(f)}. \tag{11}$$

The result is that the frequency composition of a signal below the "cutoff" (Fig. 3) will propagate faster than higher frequencies. Signals with enough bandwidth to extend into both regions will experience dispersion. It should be pointed out that the variation in permittivity extends over many decades of frequencies so that, for picosecond pulses, modal dispersion will generally be present even for very narrow lines.

B. Superconducting Dispersion and Loss

The skin-effect attenuation for a normal conductor depends strongly on the Z_0 of the transmission line and the surface resistivity of the conductor. A different situation is encountered for superconducting lines, which feature low transmission loss up to frequencies below a characteristic energy gap. However, the existence of the energy gap of a superconductor leads not only to drastic variations in the attenuation experienced by a signal, but also to significant changes in its phase velocity—a superconductor is a "perfect" conductor only for dc currents. All these features are a strong function of temperature, and above a certain critical temperature, T_c, the energy gap $\Delta(T)$ vanishes and the superconductor becomes a normal metal.

The complex surface impedance of the conductor [18] is given by

$$Z_s(f) = [j2\pi f\mu_0/\sigma]^{1/2}\coth\left\{[j2\pi f\mu_0\sigma]^{1/2}t\right\} \tag{12}$$

where σ is the electrical conductivity, and for a normal metal, simply a real constant. For a superconductor, the effect of $\Delta(T)$ is that σ is complex and frequency dependent:

$$\sigma(f) = \sigma_1(f) - j\sigma_2(f) \tag{13}$$

where σ_1 and σ_2 can be derived from the Mattis–Bardeen theory [26]:

$$\frac{\sigma_1}{\sigma_n} = \frac{2}{\hbar\omega}\int_{\Delta}^{\infty} dE\,[f(E) - f(E+\hbar\omega)] \cdot \frac{g(E)}{(E^2-\Delta^2)^{1/2}\left[(E+\hbar\omega)^2-\Delta^2\right]^{1/2}} + \frac{1}{\hbar\omega}\int_{\Delta-\hbar\omega}^{-\Delta} dE\,[1-2f(E+\hbar\omega)] \cdot \frac{g(E)}{(E^2-\Delta^2)^{1/2}\left[(E+\hbar\omega)^2-\Delta^2\right]^{1/2}} \tag{14a}$$

$$\frac{\sigma_2}{\sigma_n} = \frac{1}{\hbar\omega}\int_{\Delta-\hbar\omega,\,-\Delta}^{\Delta} dE\,[1-2f(E+\hbar\omega)] \cdot \frac{g(E)}{(\Delta^2-E^2)^{1/2}\left[(E+\hbar\omega)^2-\Delta^2\right]^{1/2}} \tag{14b}$$

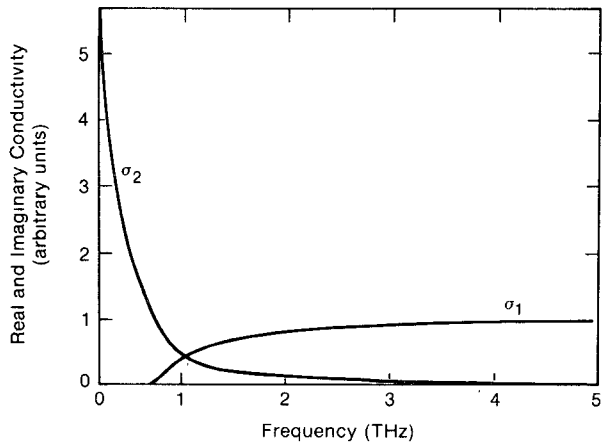

Fig. 4. Calculated frequency dependence of the normalized real and imaginary parts of conductivity for niobium at 2 K using Mattis–Bardeen theory [26].

where $g(E) = E^2 + \Delta^2 + \hbar\omega E$, $\omega = 2\pi f$, σ_n is the conductivity for the normal state of the superconductor, $\Delta = \Delta(T)$, and $f(E)$ is the Fermi–Dirac distribution function. The second integral for σ_1 is zero for $\hbar\omega < 2\Delta$, since it represents conduction due to frequencies above the gap energy, and the lower limit of integration for σ_2 changes to $-\Delta$ if $\hbar\omega > 2\Delta$. The frequency dependence for the real and imaginary parts of the conductivity is given in Fig. 4 for niobium (Nb), which has $T_c = 9.4$ K. The most distinctive feature is the large increase in real component (σ_1) and the decline of the imaginary component (σ_2) at a frequency corresponding to the energy gap.

The expressions for attenuation due to the conductors in a coplanar stripline in dB/unit length and the corresponding phase shift can be written using previous definitions:

$$\alpha_c = \mathrm{Re}[\gamma]_c = \mathrm{Re}\left[\frac{Z_s}{Z_0}\right] g_2 \tag{15}$$

$$\beta_c = \mathrm{Im}[\gamma]_c = \mathrm{Im}\left[\frac{Z_s}{Z_0}\right] g_2 \tag{16}$$

where g_2 is again given in the Appendix. From the full expressions for Z_s, Z_0, and g_2, closed-form expressions are calculated for α_c and β_c and graphically shown in Fig. 5 for an arbitrary Nb coplanar stripline at $T = 2$ K. The loss α_c [Fig. 5(a)] displays a large increase at the energy gap frequency. From (2), this attenuation, along with any dielectric contribution, directly determines $\alpha(f)$ in the propagation factor. The phase velocity, given by (10), is shown in Fig. 5(b). At lower frequencies, this quantity is constant, indicating dispersionless operation. For the broad-band signals of interest, however, the phase velocity decreases with frequency even for frequencies much less than $2\Delta/\hbar$. By (3), the imaginary contribution due to conductors, β_c, adds to the modal phase factor β_{modal} in order to give the full phase factor, $\beta(f)$, for the signal.

It should be noted that the superconducting loss factor contains a temperature dependence through the complex conductivity, and that the attenuation below the energy gap increases toward the normal value as the critical

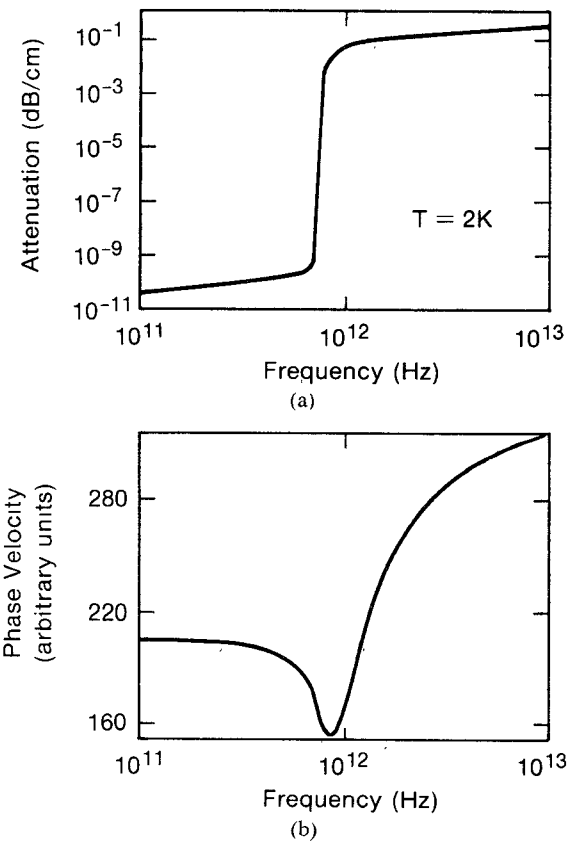

Fig. 5. Contribution of the superconducting energy gap to (a) attenuation and (b) phase velocity of Nb coplanar stripline at 2 K. Both quantities vary sharply near the energy gap frequency of 740 GHz.

temperature is approached. Therefore, from the practical point of view, one should operate superconducting transmission lines at temperatures much lower than T_c.

C. Dielectric Loss

Without attenuation, a dispersed signal would contain the same amount of energy as its input. The attenuation due to the dielectric substrate material is, in general, much less than that due to the conductors. Except in the case of very long propagation, the dielectric loss may become significant at cryogenic temperatures only when the substrate has a relatively high conductivity (such as a highly doped or narrow-band semiconductor, e.g., InSb); or it may have a dielectric resonance that follows the Debye equation or that has piezoelectric or ionic origin. For the case of substrate loss, ϵ is governed by the Kramers–Krönig relations, and the expression for α_d derived from earlier definitions is represented by [27]:

$$\alpha_d = \mathrm{Re}[\gamma]_d = 27.3 \frac{\epsilon_r}{\sqrt{\epsilon^{\mathrm{eff}}(f)}} \frac{\epsilon^{\mathrm{eff}}(f) - 1}{\epsilon_r - 1} \frac{\tan\delta}{\lambda_0} \tag{17}$$

in dB/unit length, where λ_0 is the free-space wavelength. This frequency-dependent loss factor is affected negligibly by line geometry [27].

Radiation is considered to be less significant for our lines, and has thus been omitted from the treatment, along with the negligible contribution of dielectric loss to β.

III. Model Implementation

The algorithm outlined in the previous section has been implemented in a computer program to facilitate comparison with actual experiments. Two types of input transients have been examined. The first was a normalized Gaussian input, which corresponded closely to the IBM experiments [15], [16]. A second type of input, which realistically simulates the integrating nature of a photoconductive switch, was used in our experiments, described in a later section (see also [13] and [14]). The waveform had a rising edge given by an error function matched with an exponentially rising foot in front, followed by a plateau and an exponentially falling segment.

The scheme presented in (4) calls for the use of Fourier techniques and complex algebra in order to calculate propagating waveforms. The transformations to and from the frequency domain were performed by computing the Fourier components A of a real vector of length N. The output was defined as x, where

$$x_{k+1} = \sum_{i=0}^{N-1} A_{i+1} e^{j2\pi k/N} \tag{18}$$

and $k = 0, \cdots, N-1$. The prime factors of N were found and Cooley–Tukey techniques were applied to each one.

The integration of the expressions (14a) and (14b) was also performed numerically, using a standard algorithm employing cautious adaptive Romberg extrapolation [28]. The energy gap parameter $\Delta(T)$, which was used in these expressions, has simply been tabulated versus temperature from existing graphs [29], with the value closest to the desired temperature extracted.

It was indicated in Section II-A that (8) has been extended by curve fitting to dispersion data. This was done by choosing the constants a and b associated with the normalized frequency G. A calculation for the propagation factor at one distance on a normal coplanar stripline was compared to experimental data to set the values on a and b for a line having $w = s = 50$ μm and $h = 1.0$ mm; we found $a \approx 23.5$; $b \approx 0.9$. For the other line geometry considered by us ($s = 10$ μm, $w = 5.0$ μm, and $h = 1.0$ mm, corresponding to the case of [15] and [16]), we do not have available the experimental propagation factor, and a simple geometric scaling (see e.g. [11]) was used to obtain $a \approx 260$ and $b \approx 0.9$.

IV. Examples of Computer-Simulated Results

A series of computations has been made in order to examine the propagation characteristics of short pulses on superconducting coplanar lines under different possible experimental conditions. The usefulness of the algorithm for computer-aided design of the coplanar transmission lines has also been tested. For the purpose of demonstration we use the Gaussian input pulses and Nb lines [$\Delta_{Nb}(T = 2\text{ K}) \approx 1.525$ meV—corresponding to a frequency of 740 GHz, normal resistivity $\rho_n(T \approx 10\text{ K}) = 1 \cdot 10^{-5}$ $\Omega \cdot$cm] on the silicon substrate ($\epsilon_r = 11.8$, $\tan\delta \cong 10^{-7}$). The transmission line structures considered in this section have the following parameters (see Fig. 2): $s = 10$ μm, $w = 5.0$ μm, $t = 300$ nm, and $h = 1.0$ mm.

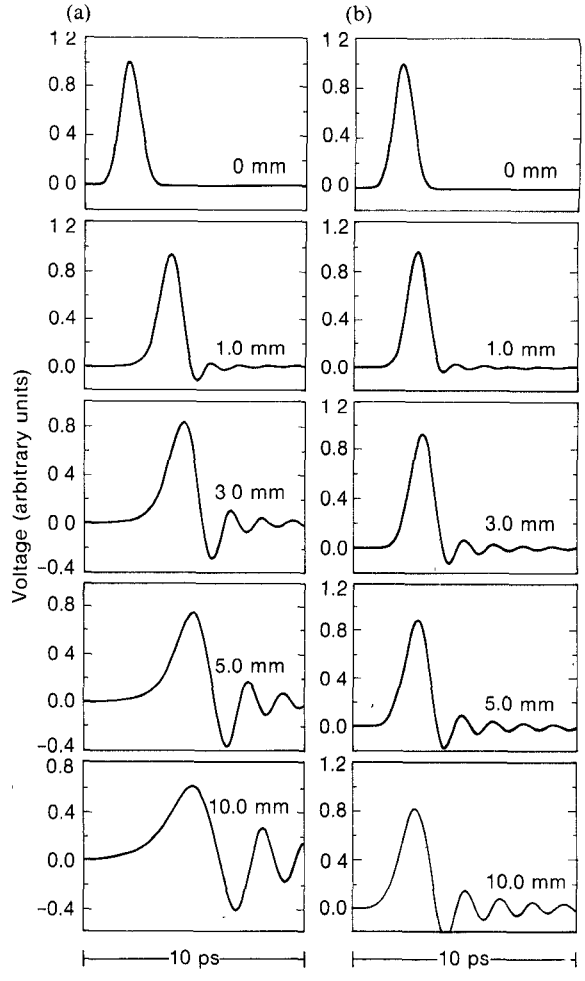

Fig. 6. Calculations for example superconducting coplanar stripline with 1 ps FWHM input for 1.0, 3.0, 5.0, and 10.0 mm propagation distances. (a) Full calculation. (b) Superconductor contribution only.

The results shown in Figs. 6–8 are presented for several pulse durations with bandwidths below and extending into the regime of frequencies affected by the energy gap. In order to determine the amount of pulse distortion due to the competing dispersion mechanisms, two sets of calculations appear in Fig. 6, one representing modal dispersion and superconducting energy gap effects considered together, and one for only the energy gap effects (TEM propagation). The pulse propagation characteristics on superconducting and normal lines are directly compared in Fig. 7. Finally, the cutoff frequency for the modal dispersion of the line has been varied by changing (Fig. 8) coplanar structure parameters.

For a 1-ps-FWHM (full width at half maximum) input pulse (Fig. 6), there is virtually no energy in frequencies above the Nb energy gap. There are, however, frequencies in the pulse that fall within the region of decreasing phase velocity shown in Figs. 3 and 5(b). This results in the dispersion seen in Fig. 6(a). In Fig. 6(b) we assume a pure TEM-wave propagation and thus the dispersion is limited to the Nb electrodes. As the pulse propagates through 1.0, 3.0, 5.0, and 10.0 mm, the higher frequencies travel more

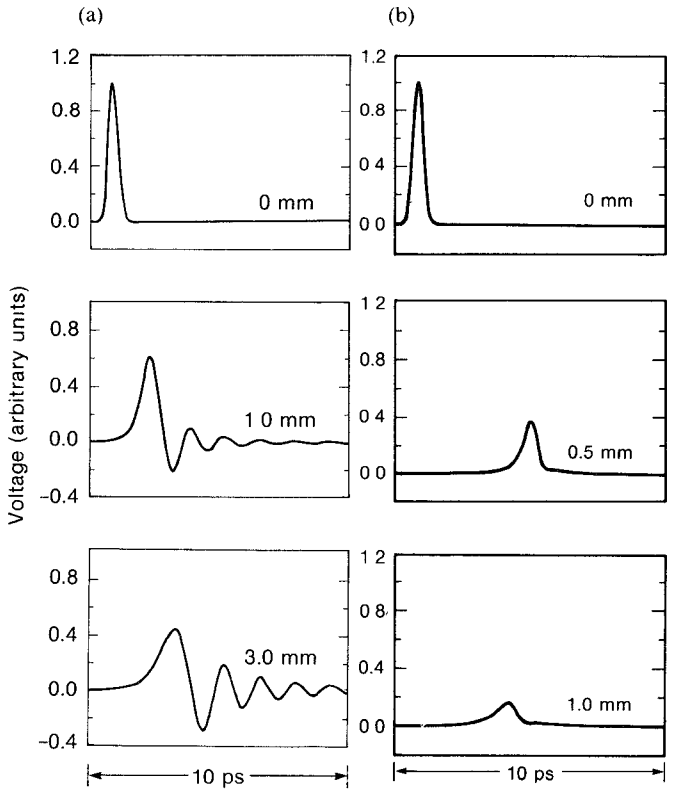

Fig. 7. Calculations with 400 fs FWHM input for example. (a) Superconducting coplanar stripline for 1.0 and 3.0 mm propagation distances. (b) Normal coplanar stripline for 0.5 and 1.0 mm propagation distances.

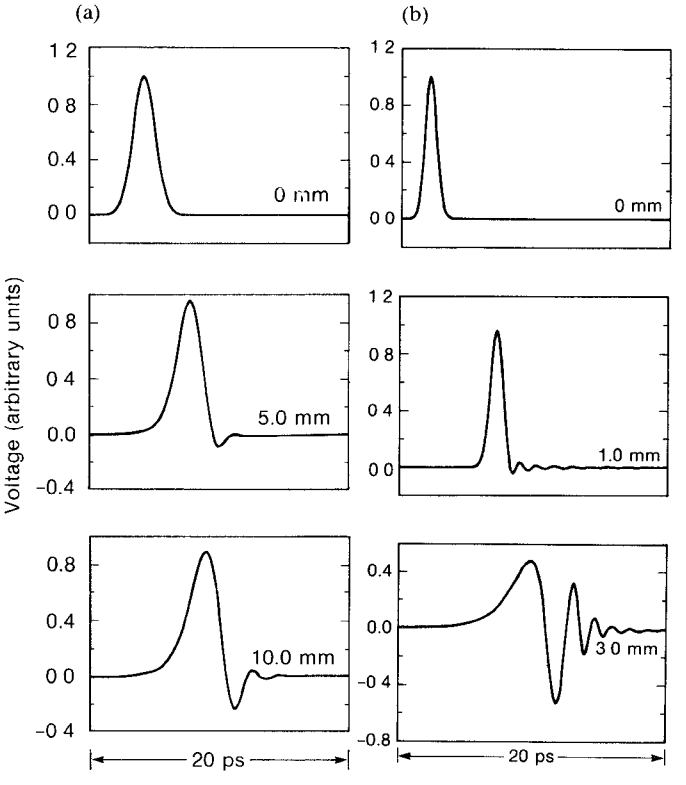

Fig. 8. (a) Calculations for example superconducting stripline with 2 ps FWHM input for 5.0 and 10.0 mm propagation distances. (b) Calculations for superconducting coplanar stripline with $w = s = 50\ \mu$m and a 1 ps FWHM input. The considerable ringing component is mainly due to modal dispersion.

slowly, resulting in longer rise time, increased pulse width, and ringing on the back of the pulse. These effects increase with transmission distance and are more pronounced for the experimentally realistic case that includes modal dispersion (see also discussion in Section V).

The input pulse in Fig. 7 has a 400-fs FWHM and a frequency content well past 1 THz. In addition to dispersion, the traces in Fig. 7(a) now display rapid attenuation above the gap frequency. Despite the short propagation distance, distortion takes place more quickly as compared with that for the waveform in Fig. 6(a). Fig. 7(b) indicates the benefit gained by the use of superconducting lines. A 400-fs-FWHM input pulse, after propagation on a normal line for only 0.5 and 1.0 mm, experiences a substantial attenuation, in addition to the usual dispersion represented by the stretched rise time. The attenuation is so severe that all ringing has been damped out, and for longer propagation distances (not shown) the pulse becomes negligibly small.

The input to Fig. 8(a) is a 2.0-ps-FWHM pulse. The propagation is calculated for correspondingly longer lengths and shows a decreased dispersion due to the almost nonexisting superconducting dispersion and the diminishing bandwidth present on the step of the permittivity curve. In fact, in this case the propagation is practically lossless, and for short distances nearly dispersion free.

To show the effect of decreasing the cutoff frequency on the modal dispersion (Fig. 8(b)), we used again a 1-ps-FWHM pulse, but on the wide coplanar line. The effect of the modal dispersion (see Fig. 3) now spreads another decade of frequencies lower, compared with the smaller lines, and the result is the drastic ringing after only 3 mm of propagation, nearly all due to modal dispersion.

V. Comparison with Experiment

The previous section has served to approximate the conditions of earlier experiments [15], as well as to indicate what results would be expected in propagating a fast transient on superconducting transmission lines. One notices the close resemblance of the model calculations to the experimental data reported [16], although no fully quantitative comparison can be made for lack of detailed information on these experiments.

As a separate, controlled check, we compared the model calculations with a series of our experiments [13], [14] where all the experimental parameters were known.

Experimentally, short pulses and broad-band signals were generated and characterized using ultrafast optical sources and the electro-optic sampling system [30]. In one experiment, transients with a 10–90 percent rise time of 1.0 ps and a relaxation time on the order of a few picoseconds were launched onto a superconducting transmission line with coplanar indium (In) striplines [$\Delta_{In}(T = 1.8\ \text{K}) \approx 0.525$ meV—corresponding to a frequency of 250 GHz, $\rho_n(T = 4.2\ \text{K}) = 2.7 \cdot 10^{-6}\ \Omega \cdot \text{cm}$] deposited on lithium tantalate ($\epsilon_r = 43$). The input pulse, with spectral components greater than the gap frequency, was simulated to begin where it was first measured (less than 75 μm from

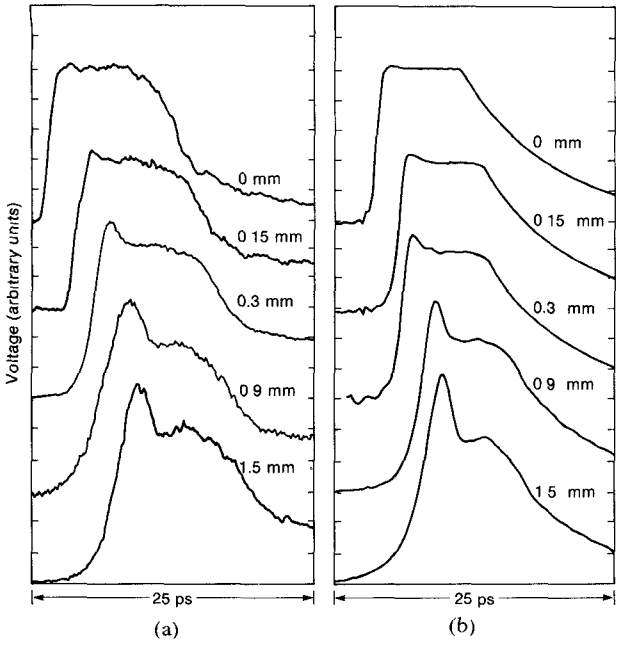

Fig. 9. Comparison of (a) experimental data and (b) calculations for propagation on In superconducting coplanar stripline on lithium tantalate substrate. Temperature was 1.8 K.

the source). This was designated as 0.0 mm, and the signal was sampled at 0.15, 0.3, 0.9, and 1.5 mm of propagation. Different characteristics were observed on the output, shown in Fig. 9: a ringing was noted on top of the plateau of the transient, and a distinctive pulse sharpening resulted as the slower, high-frequency front end of the pulse piled up on the faster moving plateau. The rise time also increased, as calculated [14].

One can observe that our computations (Fig. 9(b)) successfully simulate, both qualitatively and quantitatively, all propagation characteristics observed in the experiment (Fig. 9(a)). We want to stress that there are no completely free (adjustable) parameters in our calculations; thus the described algorithm is indeed a powerful tool for computer simulations of superconducting transmission lines operational in the microwave frequency regime.

VI. Summary

We have developed a computer algorithm to model the propagation of high-frequency signals on superconducting planar transmission lines. In addition, we have proven the accuracy of this algorithm by comparing the computed propagation with controlled experiments that measured picosecond pulse propagation on In superconducting coplanar striplines. Our calculations included the frequency dependence of phase velocity and attenuation of a signal due to modal dispersion, dielectric loss, and the complex conductivity of the superconducting lines.

An important implication of this work is that in very low loss superconducting transmission lines the dispersion becomes a dominant factor in the pulse propagation characteristics—especially after a substantial propagation distance. In order to take full advantage of the low dissipation of signals at frequencies below the energy gap in a superconducting transmission line, one needs to design the dimensions of the transmission line such that the cutoff frequency for the onset of modal dispersion is several orders of magnitude above the energy gap frequency. Alternatively, one may also use a matching dielectric superstrate on top of the transmission line to minimize modal dispersion. In such cases, the last impediment to dispersion-free propagation is the superconducting energy gap. The recent development of high-T_c superconductors [31] promises the possibility of such propagation for up to tens of terahertz.

Appendix

The geometrical factors g_1 and g_2 for coplanar striplines may be written as follows:

$$g_1 = \begin{cases} \pi\left\{\ln\left[2\dfrac{1+\sqrt{k}}{1-\sqrt{k}}\right]\right\}^{-1} & \text{for } 0 \leqslant k \leqslant 0.707 \\ \pi^{-1}\ln\left[2\dfrac{1+\sqrt{k}}{1-\sqrt{k}}\right] & \text{for } 0.707 \leqslant k \leqslant 1.0 \end{cases} \tag{A1}$$

$$g_2 = 17.34(P'/\pi s)(1+w/s) \cdot \frac{\dfrac{1.25}{\pi}\ln\dfrac{4\pi w}{t}+1+\dfrac{1.25t}{\pi w}}{\left[1+\dfrac{2w}{s}+\dfrac{1.25t}{\pi s}\left(1+\ln\dfrac{4\pi w}{t}\right)\right]^2} \tag{A2}$$

where $k = s/(s+2w)$, and

$$P' = \begin{cases} k\left[(1-\sqrt{1-k^2})(1-k^2)^{3/4}\right]^{-1} g_1^2 & \text{for } 0 \leqslant k \leqslant 0.707 \\ \left[(1-k)\sqrt{k}\right]^{-1} & \text{for } 0.707 \leqslant k \leqslant 1.0. \end{cases} \tag{A3}$$

The actual expressions for ϵ^{eff} and Z_0 utilized in our computer model further employ a correction factor, d, for the finite conductor thickness:

$$d = (1.25t/\pi)[1+\ln(4s/t)]. \tag{A4}$$

Thus, the effective linewidth is $w_t = w - d$, and the line separation becomes $s_t = s + d$. For more details the reader is referred to [19].

References

[1] J. Pustai, "Millimeter-wave transistors: The key to advanced systems," *Microwaves and RF*, vol. 26, no. 3, pp. 125–176, 1987.

[2] K. E. Meyer, D. R. Dykaar, and G. A. Mourou, "Characterization of TEGFETs and MESFETs using the electro-optic sampling technique," in *Picosecond Electronics and Optoelectronics*, G. A. Mourou, D. M. Bloom, and C.-H. Lee, Eds. Berlin: Springer-Verlag, 1985, pp. 54–57.

[3] G. A. Mourou and K. E. Meyer, "Subpicosecond electro-optic sampling using coplanar strip transmission lines," *Appl. Phys. Lett.*, vol. 45, pp. 492–494, Sept. 1984.

[4] D. R. Dykaar, R. Sobolewski, J. F. Whitaker, T. Y. Hsiang, G. A. Mourou, M. A. Hollis, B. J. Clifton, K. B. Nichols, C. O. Bozler, and R. A. Murphy, "Picosecond characterization of ultrafast phenomena: New devices and new techniques," in *Ultrafast Phenomena V*, G. R. Fleming and A. E. Siegman, Eds. Berlin: Springer-Verlag, 1986, pp. 103–106.

[5] D. R. Dykaar, R. Sobolewski, T. Y. Hsiang, and G. A. Mourou, "Response of a Josephson junction to a stepped voltage pulse," *IEEE Trans. Magn.*, vol. MAG-23, pp. 767–770, Mar. 1987.

[6] M. B. Ketchen, D. Grischkowsky, T. C. Chen, C.-C. Chi, I. N. Duling III, N. J. Halas, J.-M. Halbout, J. A. Kash, and G. P. Li, "Generation of subpicosecond electrical pulses on coplanar transmission lines," *Appl. Phys. Lett.*, vol. 48, pp. 751–753, Mar. 1986.
[7] J. A. Valdmanis and G. Mourou, "Subpicosecond electrical sampling and applications," in *Picosecond Optoelectronic Devices*, C.-H. Lee, Ed. New York: Academic Press, 1984.
[8] J. F. Whitaker, T. B. Norris, G. A. Mourou, and T. Y. Hsiang, "Pulse dispersion and shaping in microstrip lines," *IEEE Trans. Microwave Theory Tech.*, vol. MTT-35, pp. 41–47, Jan. 1987.
[9] C. J. Kryzak, S. M. Faris, K. E. Meyer, and G. A. Mourou, "Transmission line designs with a measured step response of 3 ps/cm," in *Picosecond Electronics and Optoelectronics*, G. A. Mourou, D. M. Bloom, and C.-H. Lee, Eds. Berlin: Springer-Verlag, 1985, pp. 244–248.
[10] K. K. Li, G. Arjavalingam, A. Dienes, and J. R. Whinnery, "Propagation of picosecond pulses on microwave striplines," *IEEE Trans. Microwave Theory Tech.*, vol. MTT-30, pp. 1270–1273, 1982.
[11] G. Hasnain, A. Dienes, and J. R. Whinnery, "Dispersion of picosecond pulses in coplanar transmission-lines," *IEEE Trans. Microwave Theory Tech.*, vol. MTT-34, pp. 738–741, 1986.
[12] R. L. Kautz, "Picosecond pulses on superconducting striplines," *J. Appl. Phys.*, vol. 49, pp. 308–314, 1978.
[13] T. Y. Hsiang, J. F. Whitaker, R. Sobolewski, D. R. Dykaar, and G. A. Mourou, "Propagation characteristics of picosecond electrical transients on coplanar striplines," to appear in *Appl. Phys. Lett.*
[14] J. F. Whitaker, R. Sobolewski, D. R. Dykaar, and G. A. Mourou, "Subpicosecond pulse propagation on superconducting striplines," *Jpn. J. Appl. Phys.*, vol. 26, pp. 1563–1564, 1987.
[15] C.-C. Chi, W. J. Gallagher, I. N. Duling III, D. Grischkowsky, N. J. Halas, M. B. Ketchen, and A. W. Kleinsasser, "Subpicosecond optoelectronic study of superconducting transmission-lines," *IEEE Trans. Magn.*, vol. MAG-23, pp. 1666–1669, Mar. 1987.
[16] W. J. Gallagher, C.-C. Chi, I. N. Duling III, D. Grischkowsky, N. J. Halas, M. B. Ketchen, and A. W. Kleinsasser, "Subpicosecond optoelectronic study of resistive and superconductive transmission lines," *Appl. Phys. Lett.*, vol. 50, pp. 350–352, Feb. 1987.
[17] R. L. Kautz, "Miniaturization of normal-state and superconducting striplines," *J. Res. National Bureau of Standards*, vol. 84, pp. 247–259, May 1979.
[18] R. E. Matick, *Transmission Lines for Digital and Communication Networks*. New York: McGraw-Hill, 1969, chs. 4 and 6.
[19] K. C. Gupta, R. Garg, and I. J. Bahl, *Microstrip Lines and Slotlines*. Dedham, MA: Artech House, 1979, ch. 7.
[20] T. C. Edwards, *Foundations for Microstrip Circuit Design*. Chichester: Wiley, 1981.
[21] R. Mittra and T. Itoh, "A new technique for the analysis of the dispersion characteristics of microstrip lines," *IEEE Trans. Microwave Theory Tech.*, vol. MTT-19, pp. 47–56, 1971.
[22] T. Itoh and R. Mittra, "Spectral-domain approach for calculating dispersion characteristics of microstrip lines," *IEEE Trans. Microwave Theory Tech.*, vol. MTT-21, pp. 496–499, 1973.
[23] W. J. Getsinger, "Microstrip dispersion model," *IEEE Trans. Microwave Theory Tech.*, vol. MTT-21, pp. 34–39, Jan. 1973.
[24] G. Kompa and R. Mehran, "Planar waveguide model for calculating microstrip components," *Electron. Lett.*, vol. 11, pp. 459–460, 1975.
[25] E. Yamashita, K. Atsuki, and T. Ueda, "An approximate dispersion formula of microstrip lines for computer-aided-design of microwave integrated circuits," *IEEE Trans. Microwave Theory Tech.*, vol. MTT-27, pp. 1036–1038, 1979.
[26] D. C. Mattis and J. Bardeen, "Theory of the anomalous skin effect in normal and superconducting metals," *Phys. Rev.*, vol. 111, pp. 412–417, 1958.
[27] J. R. James, P. S. Hall, and C. Wood, *Microstrip Antenna Theory and Design*. London: Peregrims for IEE, 1981, ch. 2.
[28] C. de Boor, "CADRE: An algorithm for numerical quadrature," in *Mathematical Software*, J. R. Rice, Ed. New York: Academic Press, 1971, ch. 7.
[29] M. Tinkham, *Introduction to Superconductivity*. New York: McGraw-Hill, 1975, ch. 2.
[30] J. A. Valdmanis and G. Mourou, "Subpicosecond electro-optic sampling: Principles and applications," *IEEE J. Quantum Electron.*, vol. QE-22, pp. 69–78, Jan. 1986.
[31] M. K. Wu, J. R. Ashburn, C. J. Torng, P. H. Hor, R. L. Meng, L. Gao, Z. J. Huang, Y. Q. Wang, and C. W. Chu, "Superconductivity at 93 K in a new mixed-phase Y–Ba–Cu–O compound system at ambient pressure," *Phys. Rev. Lett.*, vol. 58, pp. 908–910, 1987.

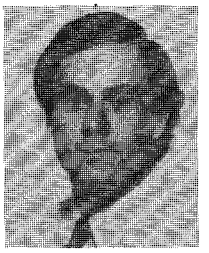

John F. Whitaker (S'84) was born in Penn Yan, NY, on March 3, 1959. He received the B.S. degree in physics from Bucknell University, Lewisburg, PA, in 1981, and the M.S. degree in electrical engineering from the University of Rochester, Rochester, NY, in 1983. He is currently a doctoral candidate in electrical engineering, studying optical electronics in the Ultrafast Science Center at the Laboratory for Laser Energetics of the University of Rochester. His research interests include superconducting transmission lines, resonant tunneling devices, and the testing of millimeter-wave MMIC's.

Mr. Whitaker is a member of the American Physical Society.

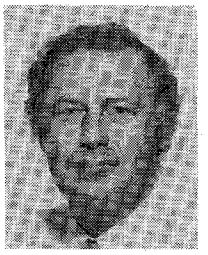

Roman Sobolewski was born in Zabrze, Poland, in 1952. He received the M.S. degree from the Warsaw Technical University, Poland, in 1975, and the Ph.D. degree from the Polish Academy of Sciences in 1983.

He was a research fellow at the Institute of Physics of the Polish Academy of Sciences, Warsaw, from 1975 to 1980, where he studied the microwave properties of Josephson tunnel junctions and worked on the national voltage standard. From 1980 to 1981 he was at the Department of Electrical Engineering of the University of Rochester, where his research focused on the study of nonequilibrium states in superconductors. After returning to Poland he rejoined the Institute of Physics. During the years 1984–1987 he worked as a Visiting Assistant Professor at the University of Rochester. Currently he is a Senior Research Associate at the Institute of Physics, Polish Academy of Sciences, as well as an Adjunct Assistant Professor at the Department of Electrical Engineering, University of Rochester. His research interests include ultrafast phenomena in semiconducting and superconducting devices, picosecond pulse propagation on superconducting and normal transmission lines, the physics of the Josephson effect and nonequilibrium superconductivity, and the electrical properties of Perovskite superconductors.

Dr. Sobolewski is a member of the American and Polish Physical Societies.

Douglas R. Dykaar, photograph and biography not available at the time of publication.

Thomas Y. Hsiang (M'81) was born in Taiwan in 1948. He received the M.A. and Ph.D. degrees from the University of California in 1973 and 1977, respectively. He was a University of California Fellow from 1971 to 1973 and a research fellow at the Ames Laboratory from 1977 to 1979, where he worked on properties of superconducting-normal metal interface.

From 1979 to 1981, he was on the faculty of the Illinois Institute of Technology, where he was a Faculty Research Fellow in 1982. He

joined the Department of Electrical Engineering at the University of Rochester in 1981 as Assistant Professor and became an Associate Professor in 1983. His current research interests include noise properties of semiconductor devices, high-speed phenomena in GaAs and superconducting devices and in transmission lines, process and device modeling, and nonequilibrium superconductivity.

Dr. Hsiang is a member of the American Physical Society.

Gerard A. Mourou was born in Albertville, France, in 1944. He received the B.S. degree from the University of Grenoble, Grenoble, France, in 1967; the Doctorat de 3ème Cycle from the University of Orsay, Orsay, France, in 1970; and the Doctorat d'Etat from the University of Paris in 1973.

From 1967 to 1970 he worked at the École Polytechnique, Paris, where he studied the spectral property of the Q-switched ruby laser. From 1970 to 1979 he was at the Université Laval, Quebec, Canada, where his interest was in the study of the picosecond kinetics of dye molecules in solutions. From 1973 to 1974 he spent a postdoctoral year at the Department of Chemistry, San Diego State University, San Diego, CA, before going back to France to join the Laboratoire d'Optique Appliquée, ENSTA-École Polytechnique, as a scientist. In 1977 he joined the Laboratory for Laser Energetics, University of Rochester, Rochester, NY, where he is now Director of the Ultrafast Science Center and Professor at the Institute of Optics. He has performed pioneering work in the development of optoelectronic sampling techniques, light-activated solid-state switching, ultra-short-pulse lasers, short-pulse electron-optical technology, and high-speed diagnostic techniques.